

Rethinking Mixup for Improving the Adversarial Transferability

Xiaosen Wang
Huawei Singular Security Lab
xiaosen@hust.edu.cn

Zeyuan Yin
Mohamed bin Zayed University of AI
zeyuan.yin@mbzuai.ac.ae

Abstract

Mixup augmentation has been widely integrated to generate adversarial examples with superior adversarial transferability when immigrating from a surrogate model to other models. However, the underlying mechanism influencing the mixup’s effect on transferability remains unexplored. In this work, we posit that the adversarial examples located at the convergence of decision boundaries across various categories exhibit better transferability and identify that *Admix* tends to steer the adversarial examples towards such regions. However, we find the constraint on the added image in *Admix* decays its capability, resulting in limited transferability. To address such an issue, we propose a new input transformation-based attack, called *Mixing the Image but Separating the gradient* (*MIST*). Specifically, *MIST* randomly mixes the input image with a randomly shifted image and separates the gradient of each loss item for each mixed image. To counteract the imprecise gradient, *MIST* calculates the gradient on several mixed images for each input sample. Extensive experimental results on the ImageNet dataset demonstrate that *MIST* outperforms existing SOTA input transformation-based attacks with a clear margin on both Convolutional Neural Networks (CNNs) and Vision Transformers (ViTs) w/o defense mechanisms, supporting *MIST*’s high effectiveness and generality.

1. Introduction

Adversarial examples, in which the imperceptible perturbations can mislead the model predictions [11, 33], reveal the extreme vulnerability of deep neural networks (DNNs) [15, 32]. It has also brought an immense threat to real-world DNNs-based applications, such as face recognition [35, 44], autonomous driving [2, 8], etc. Recently, with the increasing interest in adversarial examples, researchers have proposed tremendous adversarial attacks, such as white-box attacks [19, 27], score-based attacks [14, 18], decision-based attacks [1, 40] and transfer-based attacks [5, 41, 43].

Among various adversarial attacks, transfer-based attacks utilize the transferability of adversarial examples gen-

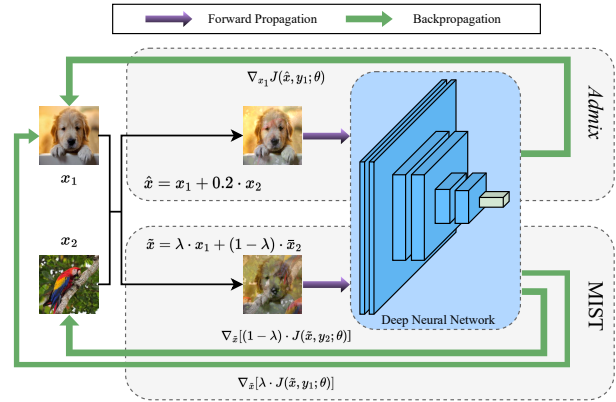


Figure 1. Illustration of the gradient calculation in *Admix* and *MIST*. The transformed image of *Admix* is visually similar to the original input image x_1 , while the one of *MIST* is a linear combination of two input images x_1 and \bar{x}_2 , in which \bar{x}_2 indicates the randomly shifted image of x_2 .

erated on the surrogate model to attack other unknown models [23]. Since transfer-based attacks do not access the target model, they are applicable to attack real-world models. However, existing adversarial attacks often exhibit superior white-box attack performance but poor transferability. To this end, numerous attacks have been proposed to boost the adversarial transferability [6, 9, 22, 39, 42, 47, 49, 55, 56].

Input transformation-based attacks, which transform the input image for gradient calculation, exhibit outstanding effectiveness in boosting the transferability and have attracted increasing attention [10, 22, 36, 38, 49]. As shown in Fig. 1, *Admix* [38] achieves outstanding performance among existing input transformation-based attacks by adding a small portion of the image from other categories to the input image for gradient calculation. In this work, we postulate and empirically validate that the adversarial examples located at the intersection of decision boundaries across various categories are more transferable using a toy two-dimensional classification task. By leveraging information from other categories, *Admix* effectively guides adversarial examples toward these convergent points of decision boundaries, which is attributed to its excellent transferability.

Nevertheless, *Admix* adopts a small portion of the image to prevent an imprecise gradient introduced by the overload of information from different categories. Such a constraint might limit the capability to steer adversarial examples towards the intersection of decision boundaries, which might limit the transferability. In this work, we identify that separating the gradient of each loss item can overcome this limitation. Based on this finding, we propose a novel input transformation-based attack, called **M**ixing the **I**mage but **S**eparating the **g**radient (MIST), to further boost the adversarial transferability. As depicted in Fig. 1, MIST distinctively mixes two input images without prioritizing one over the other. Besides, MIST employs a random shift in one image to augment the diversity of the transformed images. To prevent the imprecise information in the gradient from decaying the attack performance, MIST generates N mixed images for each input sample and calculates the average gradient across these images.

We summarize our contributions as follows:

- We hypothesize that the adversarial examples located at the intersection of decision boundaries across various categories exhibit enhanced transferability. We provide a toy example to validate this assumption and identify that *Admix* guides the adversarial examples towards such region, leading to better transferability.
- We find that the constraint on the added image in *Admix* limits the transferability and separating the gradient of each loss item can address such limitation. Based on this finding, we propose a new input transformation-based attack called MIST, which randomly mixes the input image with a randomly shifted image. To counteract the imprecise gradient, MIST calculates the gradient on N mixed images for each input sample. With a single forward propagation, MIST can calculate the gradient w.r.t. two mixed images, making it more efficient than *Admix*.
- Extensive experiments on ImageNet dataset demonstrate that MIST outperforms the winner-up approach among existing input transformation-based attacks with an average margin of 10.32% on either CNN-based or transformer-based models under various settings, showing its superiority and generality.

2. Related Work

In this section, we provide a brief overview of existing adversarial attacks and defenses.

2.1. Adversarial Attacks

Since Szegedy *et al.* [33] identified the vulnerability of DNNs against adversarial examples, numerous adversarial attacks have been proposed, such as white-box attacks [11, 19, 27], score-based attacks [14, 18], decision-based attacks [1, 40] and transfer-based attacks [5, 10, 23, 37, 49].

Transfer-based attacks have been widely investigated recently since they do not access the target model, making them applicable in the physical world.

MI-FGSM [5] introduces momentum into I-FGSM [19] to stabilize the update direction and boost transferability, which has motivated several momentum-based approaches, *e.g.*, NI-FGSM [22], VMI-FGSM [37], EMI-FGSM [39], *etc.* Ensemble attack [23, 51], which simultaneously attacks multiple deep models with different architectures, is also effective in crafting transferable adversarial examples. Besides, some regularizers [47, 57] on the intermediate features or attention heatmaps can improve the transferability. Researchers also investigate the architecture of the victim model [20, 46] or utilize the generative models to craft more transferable adversarial examples [29, 30].

Aside from the above approaches, input transformation-based attacks, which randomly transform the input image before gradient calculation, have shown remarkable effectiveness in enhancing the transferability and excellent compatibility with any existing transfer-based adversarial attacks. For instance, DIM [49] randomly resizes the input image and adds padding to obtain a transformed image with a fixed size before calculating the gradient. TIM [6] convolves the gradient of the input image with a Gaussian kernel to approximate the average gradient on several translated images. SIM [22] calculates the average gradient on ensemble scaled images using different scale factors. *Admix* [38] adds a small portion of the image from other categories to the input image for gradient calculation, in which SIM is a particular case of *Admix* without the image from other categories. AITL [52] trains a deep neural network to adaptively predict the transformations for the given image among several image transformations. SSA [26] adds Gaussian noise and randomly scales the input image in the frequency domain.

In this work, we validate that *Admix* steers the adversarial examples towards the intersection of decision boundaries across various categories, resulting in more transferable adversarial examples. However, the constraint on the added image decays its capability, which limits the transferability. Based on this finding, we propose a new input transformation-based attack to effectively utilize the information from other categories for better transferability.

2.2. Adversarial Defenses

Numerous adversarial defenses have been proposed recently to mitigate the threat of adversarial examples. For example, adversarial training [11, 27, 34, 45] injects the adversarial examples into the training set to effectively enhance the model robustness but also introduces huge computational cost and degrades the performance on benign data. On the other hand, several approaches struggle to eliminate the adversarial perturbation through various input pre-

processing strategies, such as JPEG compression [13], random Resizing and Padding (R&P) [48], or training a deep denoiser to purify the input image, namely High-level representation Guided Denoiser (HGD) [21], JPEG-based Feature Distillation (FD) [24], Neural Representation Purification (NRP) [28], *etc.* In contrast to the above empirical defenses, certified defenses offer provable defense in a given radius, such as Interval Bound Propagation (IBP) [12], CROWN [54] and Randomized Smoothing (RS) [4].

3. Approach

In this section, we rethink how to boost adversarial transferability using a toy example and detail our MIST.

3.1. Rethinking Adversarial Transferability

It is widely recognized that the objective of model training is to align with or approximate the inherent distribution of a given dataset. Considering the static nature of the data distribution, we can posit the following hypothesis regarding the decision boundary of various models with superior performance:

Assumption 1 (Similarity of decision boundary) *Given two distinct models f_1 and f_2 , which are trained on an identical dataset and yield comparable results, their respective decision boundaries exhibit a degree of similarity.*

Intuitively, the better performance achieved by the models, the higher degree of similarity in approximating the data distribution. In other words, their decision boundaries tend to be more aligned. This phenomenon underpins the rationale behind the transferability of adversarial examples across different models. Thus, the adversarial examples far away from the decision boundary around the ground-truth category tend to be more transferable.

To elucidate this concept more clearly, we devise a two-dimensional dataset encompassing three distinct categories. Then we train two linear models, denoted as f_1 and f_2 , both of which demonstrate exceptional performance. The decision boundaries of these models are graphically visualized in Fig. 2. For the data point x in the Category I, we observe that when adversarial examples are generated on model f_1 , both x_1^{adv} and x_2^{adv} emerge as viable solutions. Though they both cross over the decision boundaries of model f_1 , x_2^{adv} possesses the capability to deceive model f_2 while x_1^{adv} lacks this attribute. In other words, x_2^{adv} is more transferable than x_1^{adv} . From this sample, we can observe that regardless of variations in decision boundaries across different models, a well-trained linear model is inherently incapable of classifying data points in the intersecting regions between Categories II and III as Category I. Thus, the adversarial examples for Category I positioned at the intersection of the decision boundaries for Categories II and III exhibit the highest degree of adversarial transferability.

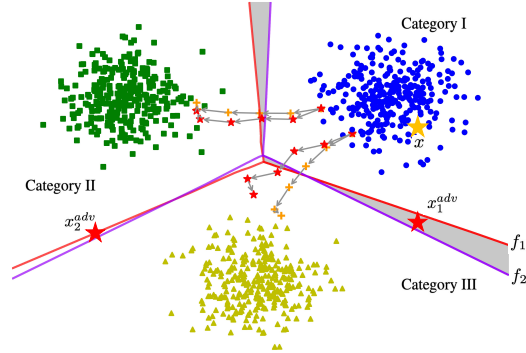


Figure 2. Visualization of decision boundaries for distinct models f_1 and f_2 trained on the two-dimensional dataset, data point x and adversarial examples x_1^{adv} and x_2^{adv} . The orange and red trajectories are the optimization paths of MI-FGSM and *Admix*.

Inspired by mixup [53], *Admix* [38] has achieved superior adversarial transferability by adopting the information of images from diverse categories. Here we delve into the underlying factors contributing to its remarkable improvement in adversarial transferability using the above toy example. Specifically, we adopt MI-FGSM [5] and *Admix* [38] to conduct untargeted attacks for a randomly sampled data point in Category I. In this process, we disregard the scale factor to solely focus on the impact of the mixup operation, which calculates the gradient as follows:

$$\bar{g}_{t+1} = \frac{1}{N} \sum_{i=1}^N \nabla_{x_t^{adv}} J(x_t^{adv} + \eta \cdot x_i, y; \theta), \quad (1)$$

where $N = 5$ is the number of sampled data points and $\eta = 0.2$ is the mix strength. In contrast to MI-FGSM, as depicted in Fig 2, the introduction of information from other categories via *Admix* notably steers the adversarial examples towards the convergence point of decision boundaries for Categories II and III. This strategic directionality of *Admix* culminates in its superior effectiveness in facilitating adversarial transferability. However, it's important to note that incorporating an excess of information from other categories can lead to less accurate gradients. This reduction in gradient precision negatively impacts the efficacy of white-box attacks, as evidenced in Tab. 1 of [38]. To mitigate this issue, *Admix* employs a mix strength $\eta = 0.2$, ensuring that the proportion of the added image remains relatively minor. This restriction, however, sometimes hinders *Admix*'s ability to consistently guide adversarial examples to the critical intersection of decision boundaries for Categories II and III (as shown in the above trajectories in Fig. 2), which limits the adversarial transferability.

It is noted that for the multi-class task and non-linear models, we can focus on the decision boundary in the vicinity of the input sample, which retains the same properties as the above example.

3.2. MIST

As discussed in Sec. 3.1, *Admix* imposes a constraint on the mix strength to address the problem where an overload of information from different categories leads to imprecise gradients. This limitation, however, inadvertently restricts the potential for adversarial transferability. This is because, in certain scenarios, a greater infusion of information from other categories is necessary to effectively direct adversarial examples towards the intersection point of decision boundaries for other categories. In this paper, we aim to explore how to lift this restriction on mix strength in *Admix* without the side effect of inducing gradient inaccuracies.

Let us go back to mixup [53], which combines two input samples (x_1, y_1) and (x_2, y_2) in the following manner:

$$\tilde{x} = \lambda \cdot x_1 + (1 - \lambda) \cdot x_2, \quad \tilde{y} = \lambda \cdot y_1 + (1 - \lambda) \cdot y_2, \quad (2)$$

where λ is a factor within the range of $[0, 1]$. Taking the cross-entropy loss function as an example, the loss can be computed as:

$$J(\tilde{x}, \tilde{y}; \theta) = \underbrace{\lambda \cdot J(\tilde{x}, y_1; \theta)}_{\text{Item I}} + \underbrace{(1 - \lambda) \cdot J(\tilde{x}, y_2; \theta)}_{\text{Item II}}. \quad (3)$$

In Eq. (3), Item II introduces much imprecise gradient w.r.t. category y_2 for the input sample x_1 . *Admix* simply eliminates Item II and sets $\lambda = 0.2$ to ensure that x_2 does not excessively impact the gradient calculation in Item I.

In this work, we argue that *mixing two images should not prioritize one image over the other to achieve better transferability*. By emphasizing the equal representation of both categories in the mixed image, we can steer the adversarial examples towards the intersection of decision boundaries for different categories. To address the issue of imprecise gradients, we propose to separate the two items in Eq. (3) when calculating the gradient w.r.t. each input sample as:

$$\begin{aligned} \nabla_{x_1} J(\tilde{x}, \tilde{y}; \theta) &= \nabla_{\tilde{x}} [\lambda \cdot J(\tilde{x}, y_1; \theta)], \\ \nabla_{x_2} J(\tilde{x}, \tilde{y}; \theta) &= \nabla_{\tilde{x}} [(1 - \lambda) \cdot J(\tilde{x}, y_2; \theta)]. \end{aligned} \quad (4)$$

To validate whether the separated gradient calculation can indeed resolve the issue of gradient imprecision and enhance adversarial transferability, we conduct an empirical experiment using Eq. (4) and *Admix* without scale. Specifically, we generate adversarial examples on ResNet-18 [15] and evaluate them on seven unknown target models, ResNet-101 [15], ResNeXt-50 [50], DenseNet-121 [17], ViT [7], PiT [16], Visformer [3], and Swin [25], as detailed in Sec. 4.1. As shown in Fig. 3, employing Eq.(4) leads to significantly improved transferable adversarial performance compared to the traditional *Admix* approach, lending credence to our hypothesis.

Based on the above analysis, we propose a new input transformation-based attack, called **Mixing the Image** but

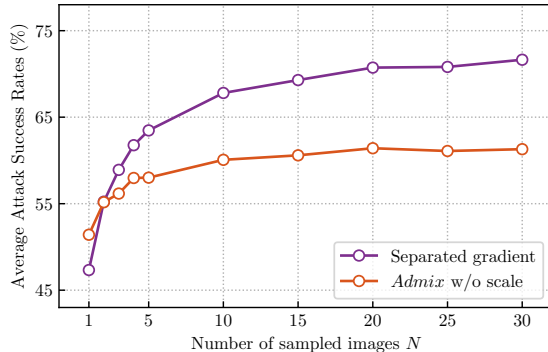


Figure 3. Average attack success rate (%) of separated gradient using Eq. (4) and *Admix* without scale, where the adversarial examples are generated on ResNet-18.

Separating the gradient (MIST). Specifically, MIST adopts Eq. (2) to generate the mixed image while simultaneously utilizing Eq. (4) to compute the gradient pertinent for each sample. Note that MIST conducts one forward propagation when calculating the gradient of two input images, making it more efficient than *Admix*. Moreover, MIST incorporates a random shift of the image x_2 to augment the diversity of mixed images. To mitigate the variability introduced by the stochastic mixup process, MIST generates N mixed images for each input sample followed by the computation of the average gradient across these images.

4. Experiments

In this section, we conduct extensive experiments on ImageNet dataset to validate the effectiveness of MIST.

4.1. Experimental Settings

Dataset. We conduct extensive experiments on 1,000 randomly sampled images belonging to 1,000 categories from the ILSVRC 2012 validation set [31], which all the corresponding models can correctly classify.

Models. To thoroughly evaluate MIST, we adopt four CNN-based networks, *i.e.*, ResNet-18, ResNet-101 [15], ResNeXt-50 [50], DenseNet-121 [17], as well as four transformer-based networks, namely ViT [7], PiT [16], Visformer [3], Swin [25]. We also study several SOTA defense approaches, namely the top-3 submissions in NIPS 2017 defense competition, *i.e.*, HGD [21], R&P [48] and NIPS-r3¹, three extra input pre-processing strategies, *i.e.*, JPEG [13], FD [24], NRP [28] and one certified defense RS [4].

Baseline. We compare MIST with five widely-adopted input transformation-based attacks, namely TIM [6], DIM [49], SIM [22], *Admix* [38], and SSA [26]. For a fair comparison, all the input transformations are integrated into MI-FGSM [5], which is aligned with previous works.

¹<https://github.com/anlthms/nips-2017/tree/master/mmd>

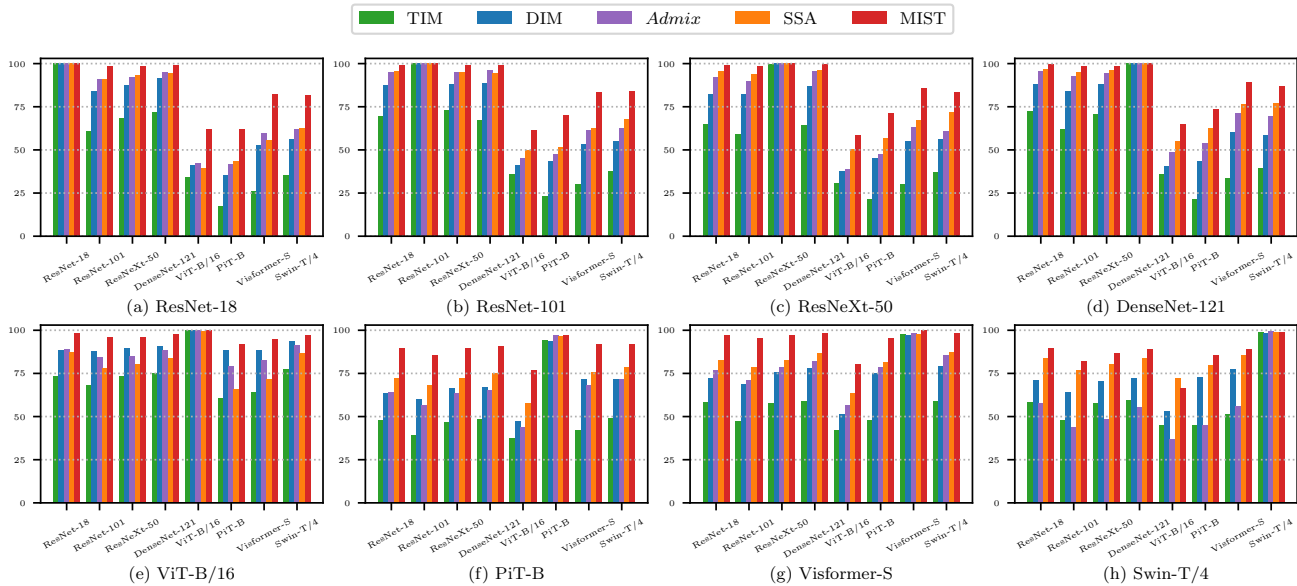


Figure 4. Attack success rates (%) on eight standardly trained models with various single input transformations, where the adversarial examples are generated on each model using the corresponding attacks.

Parameter Settings. We follow the parameter settings in *Admix* [38] with the maximum perturbation $\epsilon = 16$, the number of iteration $T = 10$, the step size $\alpha = \epsilon/T = 1.6$, and the decay factor $\mu = 1.0$ for MI-FGSM. For TIM, we utilize the Gaussian kernel with the size of 7×7 . For DIM, we set the transformation probability $p = 0.5$, and the resize rate $\rho = 1.1$. For SIM, we adopt the number of scaled copies $m = 5$ with the scaled factor $\gamma_i = 1/2^i$. For *Admix*, we follow the same scale setting in SIM and choose the number of sampled images $m_2 = 3$ with the mix strength $\eta = 0.2$. For SSA, we adopt the tuning factor $\rho = 0.5$ and the standard deviation as the perturbation budget ϵ . For MIST, we set the number of sampled images $N = 30$ with the dynamic mix strength $\lambda \in [0.2, 0.8]$.

4.2. Evaluation on Single Model

To verify the effectiveness of MIST, we adopt various single input transformation-based attacks and further integrate MIST into them to craft adversarial examples on a single model. The adversaries are crafted on the eight standardly trained models respectively, and tested on the remaining seven models to evaluate the black-box transferability.

4.2.1 Evaluation on Single Input Transformation.

We first adopt single input transformation to attack the deep models and report the attack success rates in Fig. 4, *i.e.*, the misclassification rates of the victim model on the generated adversarial examples.

Under the white-box setting, the baselines achieve near 100% attack success rate on most models except for PiT-B. On this model, *Admix* achieves the best white-box attack

performance ($\sim 95\%$) among the four baselines, indicating that mixing the information from other categories is of great benefit to boost the adversarial attack. By contrast, the attack success rates of MIST consistently reach almost 100% on all eight models, supporting its reasonable design and showing its excellent generality for various architectures.

Under the black-box setting, among four baselines, *Admix* or SSA exhibits the best attack performance when generating adversarial examples on CNN-based models. However, DIM surprisingly exhibits better attack performance when the adversarial examples are crafted on transformer-based models. This indicates the significance of thoroughly validating the attack performance on different architectures. When generating the adversarial examples on eight different models, MIST exhibits outstanding transferability compared with the baselines. In general, MIST achieves an attack success rate of 87.90% on average, which is much higher than the best baseline *Admix* (69.70%) and SSA (76.11%). On all models, MIST outperforms the winner-up approach with an average margin of 10.32%.

In summary, MIST performs much better than all the baselines under white-box and black-box settings on either CNN-based or transformer-based models, demonstrating its high effectiveness in boosting adversarial attacks and excellent generality for various architectures.

4.2.2 Evaluation on Combined Input Transformation

SIM [22], *Admix* [38] and SSA [26] can be combined with other input transformation-based attacks for better transferability. To evaluate MIST’s compatibility with these attacks, we combine MIST and MIST-SIM (combining MIST

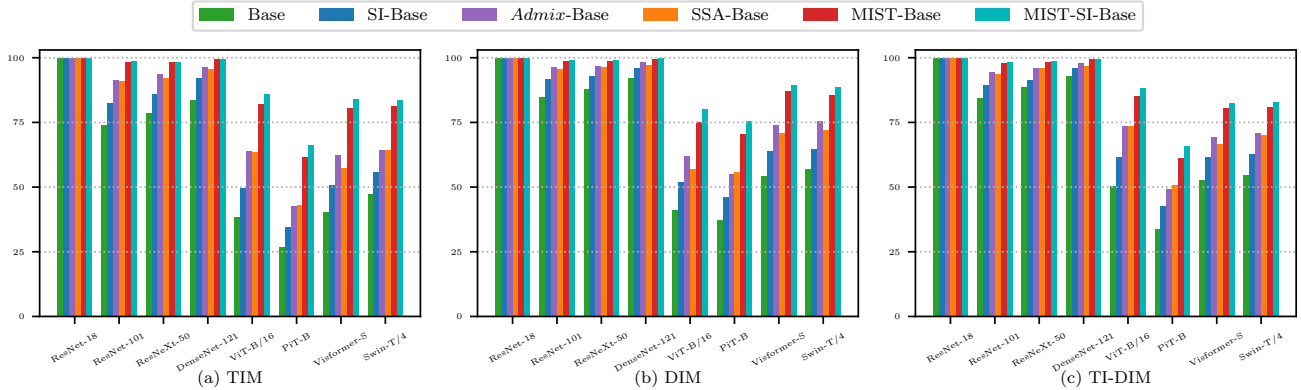


Figure 5. Attack success rates (%) on eight standardly trained models using combined input transformations. The adversarial examples are crafted on ResNet-18 using the corresponding attacks. Here **Base** indicates the basic input transformations, *i.e.*, TIM, DIM, and TI-DIM.

Ensemble	Attack	ResNet-18	ResNet-101	ResNeXt-50	DenseNet-121	ViT	PiT	ViFormer	Swin
CNNs	<i>Admix</i>	99.8*	99.9*	99.9*	100.0*	77.2	81.3	92.3	91.4
	MIST	99.8*	99.7*	99.9*	99.9*	87.1	90.4	97.4	95.9
	<i>Admix</i> -TI-DIM	99.8*	99.8*	99.8*	99.9*	89.8	78.6	90.3	90.3
	MIST-SI-TI-DIM	99.7*	99.4*	99.7*	99.9*	97.1	87.5	95.6	94.4
Transformers	<i>Admix</i>	88.7	86.4	89.3	90.3	95.4*	95.5*	96.4*	98.9*
	MIST	98.4	97.2	97.4	98.6	98.3*	98.4*	99.1*	99.0*
	<i>Admix</i> -TI-DIM	91.7	88.8	91.1	92.2	97.3*	95.9*	96.0*	98.5*
	MIST-SI-TI-DIM	98.4	97.0	98.0	98.5	98.5*	97.9*	98.9*	98.8*

Table 1. Attack success rates (%) on eight standardly trained models by *Admix* and MIST, respectively. The adversarial examples are crafted on CNN-based and Transformer-based models. * indicates white-box attacks.

with SIM) with TIM, DIM and TI-DIM to construct composite attacks, denoted as MIST (-SI)-TIM, MIST (-SI)-DIM, MIST (-SI)-TI-DIM. We report the results on ResNet-18 in Fig. 5 and the other seven models in Appendix A.

We can observe that all the attacks reach nearly 100% attack success rates on the ResNet-18, showing their high white-box attack effectiveness. Under the black-box setting, the adversarial transferability can be significantly enhanced when combined with various input transformation-based attacks, namely SIM, *Admix*, SSA, MIST and MIST-SIM. In particular, MIST outperforms the SOTA baseline *Admix* with a clear margin of 13.33%, 9.22% and 8.02% averagely, when combined with TIM, DIM and TI-DIM, respectively. More importantly, MIST-SIM, MIST combined with SIM (a special case of *Admix*), can further boost the transferability when integrated into the baselines, showing MIST’s outstanding effectiveness in crafting more transferable adversarial examples and compatibility with existing input transformation-based attacks. The results of adversarial examples crafted on the other seven models also exhibit a consistent trend, which further validates its superiority.

4.3. Evaluation on Ensemble Model

In practice, attacking multiple models simultaneously [23], *a.k.a.* ensemble attack, can significantly improve adversar-

ial transferability. Existing input transformation-based attacks are often compatible with ensemble attack. To further validate MIST’s effectiveness, we compare MIST with the best baseline *Admix* and further combine them with SI-TI-DIM/TI-DIM under the ensemble setting. As shown in Sec. 4.2, the adversarial examples exhibit transferability across different architectures, *i.e.* CNNs and transformers. Hence, we craft the adversarial examples on all CNNs or transformers and test them on the remaining models.

As shown in Tab. 1, MIST and MIST-SI-TI-DIM exhibit better white-box attack success rates than *Admix* and *Admix*-TI-DIM, especially on transformers. This also validates the rationality of MIST to separate the gradient among the mixed images. Under the black-box setting, MIST achieves much better transferability than *Admix* on various models, even better than *Admix*-TI-DIM in most cases (except for ViT). This indicates MIST’s excellent compatibility with ensemble attack and further supports the superior effectiveness of MIST. Notably, MIST-SI-TI-DIM achieves the average attack success rate of 93.7% and 98.0% when taking CNNs and Transformers as the black-box surrogate models, respectively. Such outstanding performance underscores the vulnerability of a wide range of deep models to MIST, which affirms the outstanding generality of MIST for various input transformation-based and ensemble attacks.

Attack	HGD	R&P	NIPS-r3	JPEG	FD	NRP	RS
<i>Admix</i> -TI-DIM	97.3	95.1	96.1	98.2	97.7	89.0	64.4
MIST-SI-TI-DIM	98.7	97.6	98.0	99.1	98.9	93.3	70.5

Table 2. Attack success rates (%) on seven advanced defenses by *Admix*-TI-DIM and MIST-SI-TI-DIM, respectively. The adversarial examples are crafted on eight standardly trained models.

Target model	The bound λ_{min} for mix strength					
	0	0.1	0.2	0.3	0.4	0.5
CNN	93.17	94.80	95.40	94.93	93.37	91.77
Transformer	49.50	53.00	54.15	54.33	51.20	47.20

Table 3. Average attack success rates (%) on three CNNs and four Transformers with various mix strengths. The adversarial examples are crafted on ResNet-18 and tested on the remaining models.

4.4. Evaluation on Defense Method

Until this point, the evaluations have been conducted on the standardly trained models. To mitigate the threat of adversarial examples, several adversarial defenses have been proposed. To comprehensively assess the effectiveness of MIST, we consider seven advanced defense methods, namely HGD, R&P, NIPS-r3, JPEG, FD, NRP and RS. As shown in Sec. 4.3, *Admix*-TI-DIM under the ensemble setting achieves the best attack performance among the baselines. Accordingly, we adopt *Admix*-TI-DIM and our MIST-SI-TI-DIM to generate the adversarial examples on the eight standardly trained models and test them against these defenses.

The results are summarized in Tab. 2. Though *Admix*-TI-DIM has exhibited superior attack performance on these defenses, our proposed MIST-SI-TI-DIM consistently performs better than the baseline on all the seven adopted defenses, which achieves the attack success rate of at least 70.5%. On average, MIST-SI-TI-DIM outperforms *Admix*-TI-DIM with a clear margin of 2.6%. Notably, MIST-SI-TI-DIM achieves an attack success rate of 93.3% and 70.5% on the powerful denoiser NRP or certified defense RS, respectively, exceeding those of *Admix*-SI-TI-DIM by a clear margin of 4.3% and 6.1%. These results underscore the exceptional effectiveness of our proposed MIST. More critically, the superior attack performance of MIST-SI-TI-DIM highlights the current limitations of existing defense mechanisms. It underscores an urgent need for the development of more robust defense strategies to ensure secure and reliable applications in practical scenarios.

4.5. Ablation Studies

To gain further insights into MIST, we conduct parameter and ablation studies about the mix strength, number of sampled images, and the effect of mixup and random shift.

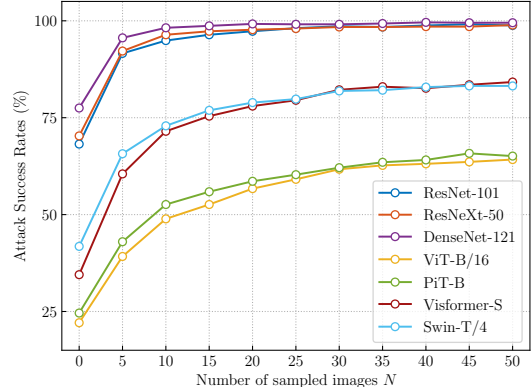


Figure 6. Attack success rates (%) on the other seven models with the adversarial examples generated by MIST on ResNet-18 using various number of sampled images N .

The impact on the mix strength. Eq. 4 shows that the direction of MIST’s gradient depends on the gradients of two mixed images and mix strength $\lambda \in [\lambda_{min}, 1 - \lambda_{min}]$. To ascertain an optimal interval for λ , we conduct experiments by varying $\lambda_{min} \in [0, 0.5]$. To avoid the uncertainty resulting from the random shift, we discard the random shift operation in this ablation experiment. As shown in Tab. 3, when λ_{min} is incrementally elevated, thereby constricting the sampling interval, the average attack success rates initially rise and subsequently decline. It suggests that the values of λ approaching 0 or 1 yield negligible mixing potency, whereas an overly restricted sampling range curtails the diversity of the mixing process. Thus, λ sampled near the extreme ends of the $[0, 1]$ interval and excessively narrow value intervals both constrain the improvement of attack success rates. To balance mix strength and sampling flexibility, we adopt $\lambda_{min} = 0.2$ in our experiments.

The impact on the number of sampled images. MIST mixes several images to construct the mixed images for gradient calculation. To ascertain the optimal number of images to mix, we conduct parameter studies for $N = 0 \rightarrow 50$ with an interval of 5. As shown in Fig. 6, MIST degenerates to MI-FGSM and is unable to exert any distinct effect when $N = 0$, which achieves the poorest attack performance. When we increase the value of N , MIST starts to be operative and the attack performance on all models stably increases, which achieves the peak around $N = 30$. Further increments in N lead to marginal enhancements in attack performance. Note that each mixed image needs one forward and two backward propagations, bringing extra computational costs. Thus, we set $N = 30$ to balance the computational cost and attack performance in our experiments.

The effect of mixup and random shift. MIST randomly shifts the sampled images and mixes them with the original input image but separates the gradient in a stan-

$Admix^\dagger$	Ablation		Target model						
	mixup	random shift	ResNet-101	ResNeXt-50	DenseNet-121	ViT	PiT	Visformer	Swin
✗	✗	✗	68.2	70.3	77.5	22.1	24.6	34.5	41.8
✓			76.7	81.6	87.5	27.5	29.5	42.8	48.7
	✓		93.5	94.9	97.8	42.1	44.2	63.8	66.5
	✓	✓	98.6	98.4	99.1	61.7	62.1	82.2	81.9

Table 4. Attack success rates (%) under different attack settings w/wo admix, mixup and random shift, respectively. The adversarial examples are crafted on ResNet-18 and tested on the other seven target models. † indicates $Admix$ without scale.

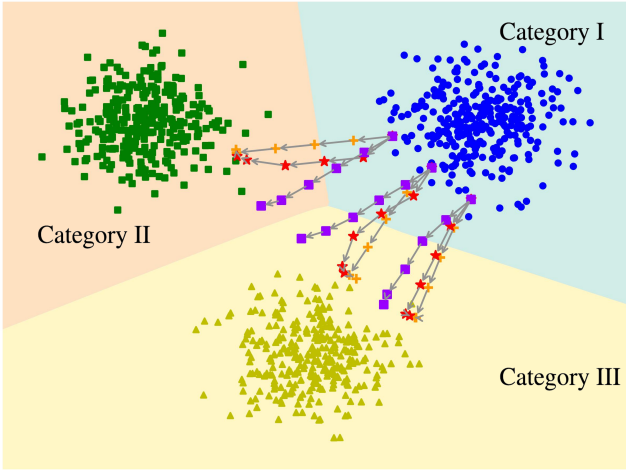


Figure 7. Visualization of optimization paths. The orange, red and purple trajectories are the optimization paths of MI-FGSM, $Admix$, and MIST, respectively.

standard mixup manner to boost the adversarial transferability. To validate whether these two components result in better transferability, we remove these components and also adopt $Admix$ without scale to generate adversarial examples on ResNet-18, then test them on the other models. The results are summarized in Tab. 4. Under the black-box setting, without mixup and random shift, MIST degenerates to MI-FGSM and achieves the poorest attack performance. Conversely, when we mix the image but separate the gradient, it can achieve much better transferability than MI-FGSM as well as $Admix$ without scale, which also mixes a small portion of images. This substantiates our hypothesis that the inherent limitations in $Admix$ impede optimal transferability. When we further adopt random shift, MIST achieves the best attack performance, supporting the necessity of random shift and rational design of our MIST.

4.6. Further Discussion

To further elucidate the mechanisms contributing to the exceptional efficacy of MIST, we visualize the optimization paths of MI-FGSM, $Admix$, and MIST using the toy exam-

ple as in Sec. 3.1. Specifically, we randomly sample several data points in Category I and record the intermediate data points along each attack’s optimization path during the generation of adversarial examples. As shown in Fig. 7, compared with MI-FGSM, $Admix$ generates the adversarial examples of Category I closer to the decision boundary between Category II and III. In comparison, MIST further enhances this trajectory, propelling the adversarial examples closer to this critical region, resulting in better adversarial transferability. This empirical evidence validates our assumption that the adversarial examples situated at the intersection of decision boundaries for other categories are more transferable. Moreover, it provides a clear illustration of how MIST successfully manipulates adversarial examples to achieve superior transferability.

5. Conclusion

In this work, we posit that adversarial examples located at the intersection of decision boundaries for other categories are more transferable. We identify that $Admix$ directs adversarial examples towards such intersections, thereby accounting for its notable efficacy. However, the constraint imposed on the incorporated image in $Admix$ prevents inaccurate gradient estimation but concurrently impairs its capacity to guide adversarial examples, consequently diminishing transferability. Based on this finding, we propose a novel input transformation-based attack called **M**ixing the **I**mage but **S**eparating the **g**radient (**MIST**). Specifically, MIST combines the input image with randomly shifted images sampled from other categories without differentiating which is primary. Subsequently, it calculates the gradients w.r.t. these two images to update their corresponding adversarial perturbation. Extensive experiments on ImageNet dataset validate its outstanding effectiveness in boosting the transferability and remarkable compatibility with other attacks under various settings. Once again, MIST certifies the superiority of adopting the information from other categories to craft more transferable adversarial examples. We hope MIST could inspire more works to utilize such information for more powerful adversarial attacks and defenses.

References

- [1] Wieland Brendel, Jonas Rauber, and Matthias Bethge. Decision-Based Adversarial Attacks: Reliable Attacks Against Black-Box Machine Learning Models. In *Proceedings of the International Conference on Learning Representations*, 2018. 1, 2
- [2] Chenyi Chen, Ari Seff, Alain L. Kornhauser, and Jianxiong Xiao. DeepDriving: Learning Affordance for Direct Perception in Autonomous Driving. In *Proceedings of the IEEE/CVF International Conference on Computer Vision*, pages 2722–2730, 2015. 1
- [3] Zhengsu Chen, Lingxi Xie, Jianwei Niu, Xuefeng Liu, Longhui Wei, and Qi Tian. Visformer: The Vision-friendly Transformer. In *Proceedings of the IEEE/CVF International Conference on Computer Vision*, pages 569–578, 2021. 4
- [4] Jeremy Cohen, Elan Rosenfeld, and J. Zico Kolter. Certified Adversarial Robustness via Randomized Smoothing. In *Proceedings of the International Conference on Machine Learning*, pages 1310–1320, 2019. 3, 4
- [5] Yinpeng Dong, Fangzhou Liao, Tianyu Pang, Hang Su, Jun Zhu, Xiaolin Hu, and Jianguo Li. Boosting Adversarial Attacks With Momentum. In *Proceedings of the IEEE/CVF Conference on Computer Vision and Pattern Recognition*, pages 9185–9193, 2018. 1, 2, 3, 4
- [6] Yinpeng Dong, Tianyu Pang, Hang Su, and Jun Zhu. Evading Defenses to Transferable Adversarial Examples by Translation-Invariant Attacks. In *Proceedings of the IEEE/CVF Conference on Computer Vision and Pattern Recognition*, pages 4312–4321, 2019. 1, 2, 4
- [7] Alexey Dosovitskiy, Lucas Beyer, Alexander Kolesnikov, Dirk Weissenborn, Xiaohua Zhai, Thomas Unterthiner, Mostafa Dehghani, Matthias Minderer, Georg Heigold, Sylvain Gelly, Jakob Uszkoreit, and Neil Houlsby. An Image is Worth 16x16 Words: Transformers for Image Recognition at Scale. In *Proceedings of the International Conference on Learning Representations*, 2021. 4
- [8] Kevin Eykholt, Ivan Evtimov, Earlene Fernandes, Bo Li, Amir Rahmati, Chaowei Xiao, Atul Prakash, Tadayoshi Kohno, and Dawn Song. Robust Physical-World Attacks on Deep Learning Visual Classification. In *Proceedings of the IEEE/CVF Conference on Computer Vision and Pattern Recognition*, pages 1625–1634, 2018. 1
- [9] Lianli Gao, Qilong Zhang, Jingkuan Song, Xianglong Liu, and Heng Tao Shen. Patch-Wise Attack for Fooling Deep Neural Network. In *Proceedings of the European Conference on Computer Vision*, pages 307–322, 2020. 1
- [10] Zhijin Ge, Xiaosen Wang, Fanhua Shang, Hongying Liu, and Yuanyuan Liu. Boosting Adversarial Transferability by Achieving Flat Local Maxima. In *Proceedings of the Advances in Neural Information Processing Systems*, 2023. 1, 2
- [11] Ian J. Goodfellow, Jonathon Shlens, and Christian Szegedy. Explaining and Harnessing Adversarial Examples. In *Proceedings of the International Conference on Learning Representations*, 2015. 1, 2
- [12] Sven Gowal, Krishnamurthy Dvijotham, Robert Stanforth, Rudy Bunel, Chongli Qin, Jonathan Uesato, Relja Arandjelovic, Timothy Arthur Mann, and Pushmeet Kohli. Scalable Verified Training for Provably Robust Image Classification. In *Proceedings of the IEEE/CVF International Conference on Computer Vision*, pages 4841–4850, 2019. 3
- [13] Chuan Guo, Mayank Rana, Moustapha Cissé, and Laurens van der Maaten. Countering Adversarial Images Using Input Transformations. In *Proceedings of the International Conference on Learning Representations*, 2018. 3, 4
- [14] Chuan Guo, Jacob R. Gardner, Yurong You, Andrew Gordon Wilson, and Kilian Q. Weinberger. Simple Black-box Adversarial Attacks. In *Proceedings of the International Conference on Machine Learning*, pages 2484–2493, 2019. 1, 2
- [15] Kaiming He, Xiangyu Zhang, Shaoqing Ren, and Jian Sun. Deep Residual Learning for Image Recognition. In *Proceedings of the IEEE/CVF Conference on Computer Vision and Pattern Recognition*, pages 770–778, 2016. 1, 4
- [16] Byeongho Heo, Sangdoon Yun, Dongyoon Han, Sanghyuk Chun, Junsuk Choe, and Seong Joon Oh. Rethinking Spatial Dimensions of Vision Transformers. In *Proceedings of the IEEE/CVF International Conference on Computer Vision*, pages 11916–11925, 2021. 4
- [17] Gao Huang, Zhuang Liu, Laurens van der Maaten, and Kilian Q. Weinberger. Densely Connected Convolutional Networks. In *Proceedings of the IEEE/CVF Conference on Computer Vision and Pattern Recognition*, pages 2261–2269, 2017. 4
- [18] Andrew Ilyas, Logan Engstrom, Anish Athalye, and Jessy Lin. Black-box Adversarial Attacks with Limited Queries and Information. In *Proceedings of the International Conference on Machine Learning*, pages 2142–2151, 2018. 1, 2
- [19] Alexey Kurakin, Ian J. Goodfellow, and Samy Bengio. Adversarial Examples in the Physical World. In *Proceedings of the International Conference on Learning Representations (Workshops)*, 2017. 1, 2
- [20] Yingwei Li, Song Bai, Yuyin Zhou, Cihang Xie, Zhishuai Zhang, and Alan L. Yuille. Learning Transferable Adversarial Examples via Ghost Networks. In *Proceedings of the AAAI Conference on Artificial Intelligence*, pages 11458–11465, 2020. 2
- [21] Fangzhou Liao, Ming Liang, Yinpeng Dong, Tianyu Pang, Xiaolin Hu, and Jun Zhu. Defense Against Adversarial Attacks Using High-Level Representation Guided Denoiser. In *Proceedings of the IEEE/CVF Conference on Computer Vision and Pattern Recognition*, pages 1778–1787, 2018. 3, 4
- [22] Jiadong Lin, Chuanbiao Song, Kun He, Liwei Wang, and John E. Hopcroft. Nesterov Accelerated Gradient and Scale Invariance for Adversarial Attacks. In *Proceedings of the International Conference on Learning Representations*, 2020. 1, 2, 4, 5
- [23] Yanpei Liu, Xinyun Chen, Chang Liu, and Dawn Song. Delving into Transferable Adversarial Examples and Black-box Attacks. In *Proceedings of the International Conference on Learning Representations*, 2017. 1, 2, 6
- [24] Zihao Liu, Qi Liu, Tao Liu, Nuo Xu, Xue Lin, Yanzhi Wang, and Wujie Wen. Feature Distillation: DNN-Oriented JPEG

- Compression Against Adversarial Examples. In *Proceedings of the IEEE/CVF Conference on Computer Vision and Pattern Recognition*, pages 860–868, 2019. 3, 4
- [25] Ze Liu, Yutong Lin, Yue Cao, Han Hu, Yixuan Wei, Zheng Zhang, Stephen Lin, and Baining Guo. Swin Transformer: Hierarchical Vision Transformer Using Shifted Windows. In *Proceedings of the IEEE/CVF International Conference on Computer Vision*, pages 9992–10002, 2021. 4
- [26] Yuyang Long, Qilong Zhang, Boheng Zeng, Lianli Gao, Xianglong Liu, Jian Zhang, and Jingkuan Song. Frequency domain model augmentation for adversarial attack. In *Proceedings of the European Conference on Computer Vision*, pages 549–566, 2022. 2, 4, 5
- [27] Aleksander Madry, Aleksandar Makelov, Ludwig Schmidt, Dimitris Tsipras, and Adrian Vladu. Towards Deep Learning Models Resistant to Adversarial Attacks. In *Proceedings of the International Conference on Learning Representations*, 2018. 1, 2
- [28] Muzammal Naseer, Salman H. Khan, Munawar Hayat, Fahad Shahbaz Khan, and Fatih Porikli. A Self-supervised Approach for Adversarial Robustness. In *Proceedings of the IEEE/CVF Conference on Computer Vision and Pattern Recognition*, pages 259–268, 2020. 3, 4
- [29] Muzammal Naseer, Salman H. Khan, Munawar Hayat, Fahad Shahbaz Khan, and Fatih Porikli. On Generating Transferable Targeted Perturbations. In *Proceedings of the IEEE/CVF International Conference on Computer Vision*, pages 7688–7697, 2021. 2
- [30] Omid Poursaeed, Isay Katsman, Bicheng Gao, and Serge J. Belongie. Generative Adversarial Perturbations. In *Proceedings of the IEEE/CVF Conference on Computer Vision and Pattern Recognition*, pages 4422–4431, 2018. 2
- [31] Olga Russakovsky, Jia Deng, Hao Su, Jonathan Krause, Sanjeev Satheesh, Sean Ma, Zhiheng Huang, Andrej Karpathy, Aditya Khosla, Michael S. Bernstein, Alexander C. Berg, and Li Fei-Fei. ImageNet Large Scale Visual Recognition Challenge. *International journal of computer vision*, 115(3): 211–252, 2015. 4
- [32] Karen Simonyan and Andrew Zisserman. Very Deep Convolutional Networks for Large-Scale Image Recognition. In *Proceedings of the International Conference on Learning Representations*, 2015. 1
- [33] Christian Szegedy, Wojciech Zaremba, Ilya Sutskever, Joan Bruna, Dumitru Erhan, Ian J. Goodfellow, and Rob Fergus. Intriguing Properties of Neural Networks. In *Proceedings of the International Conference on Learning Representations*, 2014. 1, 2
- [34] Florian Tramèr, Alexey Kurakin, Nicolas Papernot, Ian J. Goodfellow, Dan Boneh, and Patrick D. McDaniel. Ensemble Adversarial Training: Attacks and Defenses. In *Proceedings of the International Conference on Learning Representations*, 2018. 2
- [35] Hao Wang, Yitong Wang, Zheng Zhou, Xing Ji, Dihong Gong, Jingchao Zhou, Zhifeng Li, and Wei Liu. CosFace: Large Margin Cosine Loss for Deep Face Recognition. In *Proceedings of the IEEE/CVF Conference on Computer Vision and Pattern Recognition*, pages 5265–5274, 2018. 1
- [36] Kunyu Wang, Xuanran He, Wenxuan Wang, and Xiaosen Wang. Boosting Adversarial Transferability by Block Shuffle and Rotation. *arXiv preprint arXiv:2308.10299*, 2023. 1
- [37] Xiaosen Wang and Kun He. Enhancing the Transferability of Adversarial Attacks Through Variance Tuning. In *Proceedings of the IEEE/CVF Conference on Computer Vision and Pattern Recognition*, pages 1924–1933, 2021. 2
- [38] Xiaosen Wang, Xuanran He, Jingdong Wang, and Kun He. Admix: Enhancing the Transferability of Adversarial Attacks. In *Proceedings of the IEEE/CVF International Conference on Computer Vision*, pages 16138–16147, 2021. 1, 2, 3, 4, 5
- [39] Xiaosen Wang, Jiadong Lin, Han Hu, Jingdong Wang, and Kun He. Boosting Adversarial Transferability through Enhanced Momentum. In *Proceedings of the British Machine Vision Conference*, page 272, 2021. 1, 2
- [40] Xiaosen Wang, Zeliang Zhang, Kangheng Tong, Dihong Gong, Kun He, Zhifeng Li, and Wei Liu. Triangle Attack: A Query-Efficient Decision-Based Adversarial Attack. In *Proceedings of the European Conference on Computer Vision*, pages 156–174, 2022. 1, 2
- [41] Xiaosen Wang, Kangheng Tong, and Kun He. Rethinking the Backward Propagation for Adversarial Transferability. In *Proceedings of the Advances in Neural Information Processing Systems*, 2023. 1
- [42] Xiaosen Wang, Zeliang Zhang, and Jianping Zhang. Structure Invariant Transformation for better Adversarial Transferability. In *Proceedings of the IEEE/CVF International Conference on Computer Vision*, pages 4607–4619, 2023. 1
- [43] Xingxing Wei, Siyuan Liang, Ning Chen, and Xiaochun Cao. Transferable Adversarial Attacks for Image and Video Object Detection. In *Proceedings of the International Joint Conference on Artificial Intelligence*, pages 954–960, 2019. 1
- [44] Yandong Wen, Kaipeng Zhang, Zhifeng Li, and Yu Qiao. A Discriminative Feature Learning Approach for Deep Face Recognition. In *Proceedings of the European Conference on Computer Vision*, pages 499–515, 2016. 1
- [45] Eric Wong, Leslie Rice, and J. Zico Kolter. Fast is Better than Free: Revisiting Adversarial Training. In *Proceedings of the International Conference on Learning Representations*, 2020. 2
- [46] Dongxian Wu, Yisen Wang, Shu-Tao Xia, James Bailey, and Xingjun Ma. Skip Connections Matter: On the Transferability of Adversarial Examples Generated with ResNets. In *Proceedings of the International Conference on Learning Representations*, 2020. 2
- [47] Weibin Wu, Yuxin Su, Michael R. Lyu, and Irwin King. Improving the Transferability of Adversarial Samples With Adversarial Transformations. In *Proceedings of the IEEE/CVF Conference on Computer Vision and Pattern Recognition*, pages 9024–9033, 2021. 1, 2
- [48] Cihang Xie, Jianyu Wang, Zhishuai Zhang, Zhou Ren, and Alan L. Yuille. Mitigating Adversarial Effects Through Randomization. In *Proceedings of the International Conference on Learning Representations*, 2018. 3, 4

- [49] Cihang Xie, Zhishuai Zhang, Yuyin Zhou, Song Bai, Jianyu Wang, Zhou Ren, and Alan L. Yuille. Improving Transferability of Adversarial Examples With Input Diversity. In *Proceedings of the IEEE/CVF Conference on Computer Vision and Pattern Recognition*, pages 2730–2739, 2019. [1](#), [2](#), [4](#)
- [50] Saining Xie, Ross B. Girshick, Piotr Dollár, Zhuowen Tu, and Kaiming He. Aggregated Residual Transformations for Deep Neural Networks. In *Proceedings of the IEEE/CVF Conference on Computer Vision and Pattern Recognition*, pages 5987–5995, 2017. [4](#)
- [51] Yifeng Xiong, Jiadong Lin, Min Zhang, John E. Hopcroft, and Kun He. Stochastic Variance Reduced Ensemble Adversarial Attack for Boosting the Adversarial Transferability. In *Proceedings of the IEEE/CVF Conference on Computer Vision and Pattern Recognition*, pages 14963–14972, 2022. [2](#)
- [52] Zheng Yuan, Jie Zhang, and Shiguang Shan. Adaptive Image Transformations for Transfer-Based Adversarial Attack. In *Proceedings of the European Conference on Computer Vision*, pages 1–17, 2022. [2](#)
- [53] Hongyi Zhang, Moustapha Cissé, Yann N. Dauphin, and David Lopez-Paz. Mixup: Beyond Empirical Risk Minimization. In *Proceedings of the International Conference on Learning Representations*, 2018. [3](#), [4](#)
- [54] Huan Zhang, Tsui-Wei Weng, Pin-Yu Chen, Cho-Jui Hsieh, and Luca Daniel. Efficient Neural Network Robustness Certification with General Activation Functions. In *Proceedings of the Advances in Neural Information Processing Systems*, pages 4944–4953, 2018. [3](#)
- [55] Jianping Zhang, Weibin Wu, Jen-tse Huang, Yizhan Huang, Wenxuan Wang, Yuxin Su, and Michael R. Lyu. Improving Adversarial Transferability via Neuron Attribution-based Attacks. In *Proceedings of the IEEE/CVF Conference on Computer Vision and Pattern Recognition*, pages 14973–14982, 2022. [1](#)
- [56] Yaoyuan Zhang, Yu-an Tan, Tian Chen, Xinrui Liu, Quanxin Zhang, and Yuanzhang Li. Enhancing the Transferability of Adversarial Examples with Random Patch. In *Proceedings of the International Joint Conference on Artificial Intelligence*, pages 1672–1678, 2022. [1](#)
- [57] Wen Zhou, Xin Hou, Yongjun Chen, Mengyun Tang, Xi-angqi Huang, Xiang Gan, and Yong Yang. Transferable Adversarial Perturbations. In *Proceedings of the European Conference on Computer Vision*, pages 471–486, 2018. [2](#)

A. Additional Evaluations on combined input transformation

In Sec. 4.2, we provide the attack results of the adversarial examples generated by various combined input transformation-based attacks on ResNet-18. To further validate the compatibility of MIST, we generate adversarial examples on the remaining seven source models, *i.e.*, ResNet-101, ResNeXt-50, DenseNet-121, ViT, PiT, Visformer as well as Swin and test them on the other models.

The results are summarized in Fig. 8. Under the white-box setting, the baselines can achieve the attack success rate of nearly 100% on five models (*i.e.*, ResNet-101, ResNeXt-50, DenseNet-121, ViT, Swin) but exhibit slightly poor performance on the other two models (*i.e.*, PiT, Visformer). On the contrary, our proposed MIST consistently achieves the attack success rate of nearly 100% on all the models when combined with various input transformations, showing its stability and generality for different architectures. Under the black-box setting, MIST combined with various input transformations achieves significantly better attack performance than that combined with other baselines on all the models. Also, when integrating MIST-SIM into these input transformation-based attacks, we could obtain the best attack performance under the same setting. These results are consistent with that of adversarial examples generated on ResNet-18 as shown in Sec. 4.2. Once again, these superior results demonstrate MIST’s outstanding effectiveness in boosting adversarial attacks and generality for different architectures.



Figure 8. Attack success rates (%) on eight standardly trained models with the adversarial examples generated on the seven source models using different combined input transformations.